

# A Wideband Differentially Fed Dual-Polarized Antenna With Wideband Harmonic Suppression

Le-Hu Wen, Steven Gao, Qi Luo, Qingling Yang, Wei Hu, Yingzeng Yin, Xiaofei Ren, and Jian Wu

**Abstract**—A wideband differentially fed dual-polarized antenna with wideband harmonic suppression is presented. The radiating structure is composed of open slots, stair-shaped strips, and a square patch. To realize symmetrical radiation and low cross-polarization for orthogonal polarizations, eight open slots are etched on the four corners of the square patch. Stair-shaped strips are not only used to excite the open slots, but also introduce the monopole resonance. In addition, patch resonance is excited on the center square patch. To match these different resonances, shorted microstrip lines are utilized to achieve the wide impedance bandwidth. Moreover, compact stepped impedance resonators are elaborately introduced on the top of the patch to achieve wideband harmonic suppression without any increase of the antenna footprint. To verify the design method, the proposed antenna is designed, fabricated, and measured. Measured results demonstrate that the proposed antenna has the impedance bandwidth of 1.70-2.81 GHz for  $S_{dd11} < -15$  dB with high isolation of 39 dB. Moreover, wideband harmonic suppression is measured from 3 GHz to 9 GHz with the  $S_{dd11}$  higher than  $-2.2$  dB and the corresponding harmonic gain lower than  $-5.3$  dBi. In addition, stable gain of 7.2-7.9 dBi and beamwidth of 63-71° are achieved for base station applications.

**Index Terms**—Broadband, differentially fed antenna, harmonic suppression, stepped impedance resonator.

## I. INTRODUCTION

Owing to the advantages of the reduced multi-path fading effect and the increased communication capacity, dual-polarized antennas have been widely applied in many wireless communication systems, such as base stations, satellites, radars, etc. With the fast development of these communication systems [1]-[2], higher requirements are put forward to guarantee the communication quality, including wide impedance bandwidth, high port isolation, low cross-polarization, and even high harmonic suppression. Recently, more and more differential devices and circuit systems are researched owing to their advantages of high common mode rejection and low noise level [3]. However, if the traditional single-ended antennas are utilized in the differential circuit systems, out-of-phase baluns or power dividers will be inserted, and additional insertion loss and impedance mismatching will be introduced. Therefore, it is necessary to directly research differentially fed antennas for these differential circuit systems.

To obtain wideband impedance bandwidth, many different techniques are utilized to design differentially fed patch antennas [4]-[11]. However, due to the low profile and planar configuration, patch antennas normally face the problem of limited bandwidth, which is difficult to meet the bandwidth requirement for base stations. Because of the wideband requirement for 2G/3G/4G base stations (1.7-2.7 GHz), dipoles are normally utilized to design

wideband dual-polarized antennas [12]-[18]. These antennas normally can meet the bandwidth requirement for base stations, including the low cross-polarization, stable gain and beamwidth. However, few of them consider the harmonic suppression of the base station antennas, which can reduce the efficiency of the power amplifiers in the transmitter, and cause serious electromagnetic interferences to the other wireless systems [19]. In addition, the undesired harmonic radiations can be received by the receiver, reduce the sensitivity of the receiver, and even congest the receiver with strong magnitude [20]. Therefore, it is necessary to develop wideband base station antennas with harmonic suppression characteristic.

In this communication, a wideband differentially fed dual-polarized antenna by using open slots, monopoles, and a square patch is presented with wideband harmonic suppression. Symmetrical eight open slots are etched on the four corners of the center square patch to realize symmetrical and low cross-polarized radiation. Stair-shaped strips are used to excite the open slots and also radiate as the monopoles. The center square patch not only introduces the patch resonance, but also leaves space for the newly incorporated function of harmonic suppression. Shorted microstrip lines are introduced to match these three different resonances with wide impedance bandwidth. To get wideband suppression to the harmonic radiation from the antenna, compact stepped impedance resonators are elaborately introduced on the top of the patch without any increase of the footprint of the antenna. The proposed antenna was finally designed, fabricated, and measured. Both the measured and simulated results prove that the proposed antenna has the impedance bandwidth of 1.70-2.81 GHz with very high isolation of 39 dB. Moreover, compared to the traditional designed base station antennas, wideband harmonic suppression from 3 GHz to 9 GHz is measured with the reflection coefficient higher than  $-2.2$  dB and related undesired harmonic gain lower than  $-5.3$  dBi. In addition, stable antenna gain and radiation patterns are achieved for base station applications.

## II. DUAL-POLARIZED ANTENNA

### A. Antenna Configuration

The configuration of the proposed dual-polarized antenna is shown in Fig. 1, which is composed of a square substrate printed with antenna radiator, four coaxial cables as the antenna differential feeds, and a square copper sheet as the antenna reflector. A low-cost substrate of Rogers 4003C with the relative dielectric permittivity of 3.55 and the thickness of 0.813 mm is used to fabricate the antenna. The length of the square reflector is 140 mm. Differential pairs of port 1, port 2, port 3, and port 4 are used to excite the dual-polarized antenna for  $\pm 45^\circ$  polarizations. To facilitate the calculation of the differentially driven antenna, the pair of single-ended port 1 and port 2 is defined as the differential port d1, and the pair of single-ended port 3 and port 4 is defined as the differential port d2. Accordingly, the S-parameters of the differentially driven antenna can be obtained by using the single-ended four-port S-parameters [3]. In addition, because the antenna is designed for base station applications, to

This work was supported in part by China Research Institute of Radiowave Propagation, in part by EPSRC grants EP/N032497/1 and EP/P015840/1, and in part by China Scholarship Council.

L.-H. Wen, S. Gao, Q. Luo, and Q. Yang are with the School of Engineering and Digital Arts, University of Kent, Canterbury, CT2 7NT, U.K. (e-mail: lw347@kent.ac.uk)

W. Hu and Y. Yin are with the National Key Laboratory of Antennas and Microwave Technology, Xidian University, Xian, 710071, China.

X. Ren and J. Wu are with the Innovation and Research Center, China Research Institute of Radiowave Propagation, Qingdao, 266107, China..

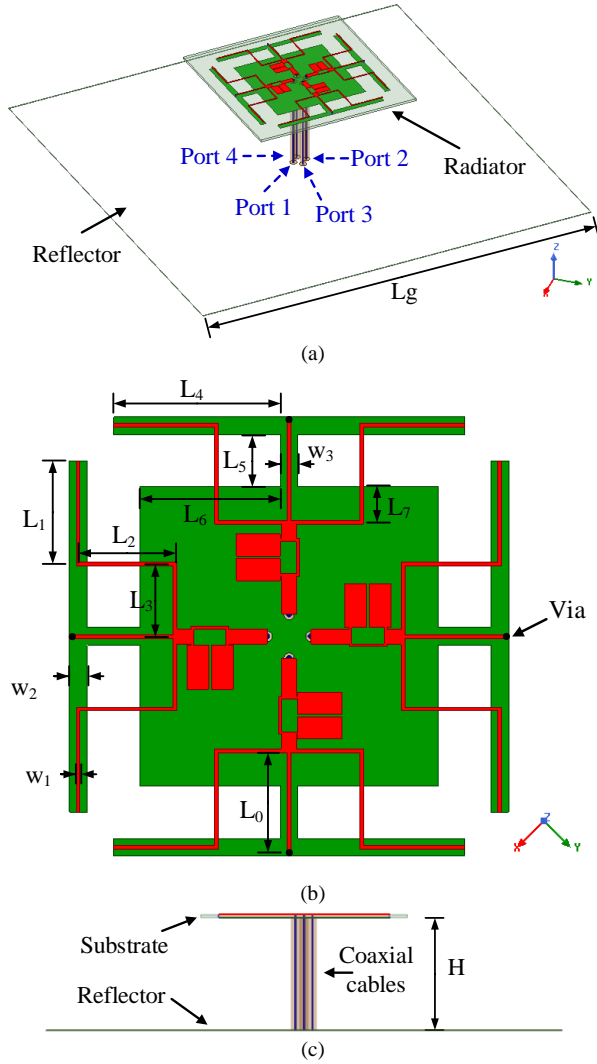


Fig. 1. Configuration of the proposed dual-polarized antenna. (a) Isometric view. (b) Top view of the antenna radiator. (c) Side view. (Detailed parameters of the proposed dual-polarized antenna:  $L_g=140$  mm,  $L_0=11.5$  mm,  $L_1=11.75$  mm,  $L_2=11$  mm,  $L_3=8.25$  mm,  $L_4=20$  mm,  $L_5=6$  mm,  $L_6=16$  mm,  $L_7=4$  mm,  $w_1=0.4$  mm,  $w_2=2$  mm,  $w_3=2$  mm,  $H=33$  mm.)

analyze the radiation patterns for  $\pm 45^\circ$  polarizations, the  $xz$  plane in the figure is defined as the horizontal plane (H-plane), and the  $yz$  plane is defined as the vertical plane (V-plane).

Fig. 1 (b) shows the details of the antenna radiator on the top and bottom layers of the substrate. In the figure, the top layer is depicted in red color, and the bottom layer is depicted in green color. On the top layer, there are eight stair-shaped narrow strips, four narrow shorted strips, and four stepped impedance resonators. While on the bottom layer, there is a square patch connected by four T-shaped stubs. With the proposed configuration, three different resonances are developed. First, eight open slots formed by the T-shaped strips and the square patch are excited and radiate as the slot resonance. Then, stair-shaped narrow strips are utilized to feed the open slots and also radiate as the monopoles. In addition, the square patch at the center of the bottom layer is also resonated and radiated. To get the wide impedance bandwidth, four shorted microstrip lines are introduced to match the three different resonances to the feed coaxial cables. Furthermore, to suppress the harmonic radiations of the antenna, four compact stepped impedance resonators are elaborately integrated onto the top of the patch to achieve wideband harmonic

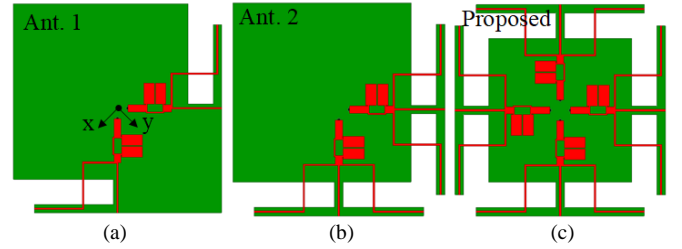


Fig. 2. Evolution process of the proposed differentially fed dual-polarized antenna. (a) Ant. 1. (b) Ant. 2. (c) Proposed antenna.

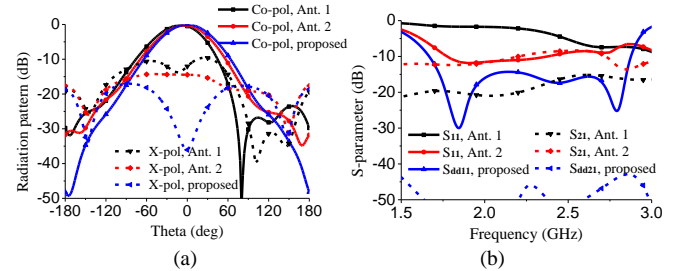


Fig. 3. Simulated results of the antennas in the evolution process. (a) Radiation patterns at 2.2 GHz in V-plane. (b) S-parameters.

suppression without any increase of the antenna footprint. Detailed working principles of the antenna will be discussed in the following sections.

Fig. 1 (c) shows the side view of the differentially fed antenna. Four coaxial cables are used to feed the antenna. Note that the outer conductors of the cables are soldered to the bottom square patch, while the inner conductors are soldered to the top feed microstrip lines. The height from the radiator to the reflector is 33 mm. All the simulation in this work are obtained from the 3D electromagnetic simulation software ANSYS HFSS. The detailed optimized parameters of the antenna are listed in caption of Fig. 1.

## B. Antenna Design

It is normally difficult to realize symmetrical radiation for dual-polarization by using single open slot. Therefore, eight symmetrical open slots are etched on the four corners of a square patch to obtain symmetrical radiation pattern and also low cross-polarization. To illustrate the evolution process of the presented antenna, reference antennas in the evolution are shown in Fig. 2. In the figure, Ant. 1 in Fig. 2 (a) has two open slots, which are etched on the two opposite corners of the square patch. Two feed lines are orthogonally arranged for dual-polarization. In Fig. 2 (b), two more symmetrical open slots are added in Ant. 2. In Fig. 2 (c), eight open slots are etched on the four corners of the patch to obtain the entire structural symmetry as the proposed antenna, and the antenna is fed by the differential fed ports.

Fig. 3 shows the corresponding simulated radiation patterns and the S-parameters of the reference antennas in the evolution process. Although all the reference antennas are symmetrical in V-plane, unsymmetrical radiation patterns are still observed for Ant. 1 and Ant. 2 in V-plane. In Fig. 3 (a), Ant. 1 has the worst radiation patterns, including the unsymmetrical co-polarization and the poorest cross-polarization level. After incorporating the other two symmetrical slots for Ant. 2, the symmetry of the co-polarized radiation pattern is a little improved and the cross-polarization level is reduced to some extent. However, the radiation patterns of Ant. 1 and Ant. 2 are still worse than the proposed antenna. The main reason for these results is the strong reflections at the two input ports and the poor isolations between the two input ports for these two

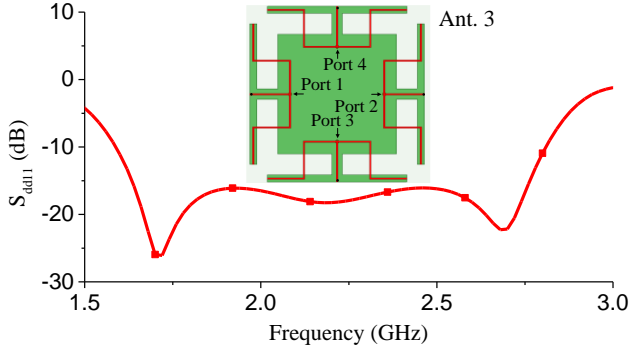


Fig. 4. Simulated  $S_{dd11}$  of the simplified reference antenna (Ant. 3).

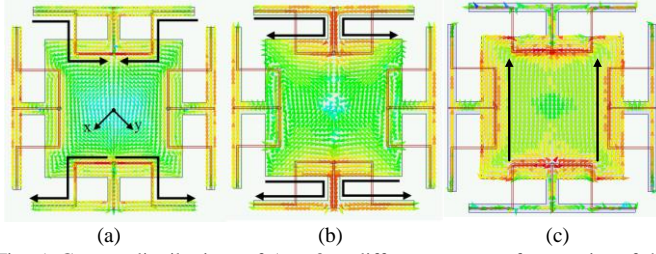


Fig. 5. Current distributions of Ant. 3 at different resonant frequencies of the reference antenna. (a) 2.68 GHz. (b) 2.18 GHz. (c) 1.72 GHz.

reference antennas, and these S-parameters are shown in Fig. 3 (b). Compared to Ant. 1, worse isolation is observed for Ant. 2. This is caused by the strong coupling between the two radiating slots at the bottom right corner of the square patch. As for the radiation patterns in H-plane, they will be more seriously affected, including the asymmetry of the co-polarized radiation pattern and poor cross-polarization levels, which are caused by the asymmetry of the antenna structure in this plane. Therefore, to get symmetrical radiation patterns in both H-plane and V-plane, eight open slots are etched symmetrically on the four corners of the patch for the proposed antenna. By using the differentially fed method, orthogonal polarizations are excited with symmetrical radiation patterns and very low cross-polarization level in the broadside direction. Furthermore, the simulated S-parameters in Fig. 3 (b) also show that the proposed antenna has the high port isolation ( $>45$  dB) and the low reflection coefficient ( $<-15$  dB) with three reflection zeroes within the bandwidth (1.68-2.8 GHz).

### C. Multi-Resonance Characteristic

The proposed antenna has the multi-resonance characteristic with three different resonances, including the open slot resonance, the monopole resonance, and the patch resonance. In the configuration of the antenna, eight symmetrical open slots are introduced at the four edges of the center patch. Eight stair-shaped strips working as the monopoles are used to excite the eight open slots. The center square patch is also elaborately excited by optimizing the parameters of the antenna. To illustrate the working principle of the three different resonances, a simplified reference antenna (Ant. 3) is investigated, and it is inset into Fig. 4. Different from the proposed antenna, four integrated stepped impedance resonators are removed from the top layer to clearly show the different resonances of the antenna. In addition, the antenna input ports are moved to the feed lines to directly reflect the input impedance of antenna. Other configuration parameters of Ant. 3 are the same as the proposed antenna. The simulated reflection coefficient of Ant. 3 is shown in Fig. 4. Three reflection zeroes are clearly observed at 1.72 GHz, 2.18 GHz, and 2.68 GHz, and these different reflection zeroes represent three different resonances.

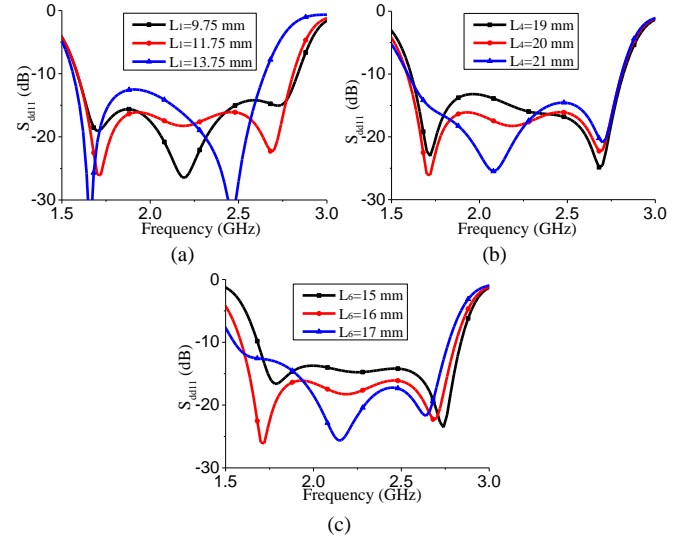


Fig. 6. Parameters study of the different resonances of the reference antenna. (a)  $L_1$ . (b)  $L_4$ . (c)  $L_6$ .

Fig. 5 shows the current distributions of Ant. 3 at these different resonant frequencies. In Fig. 5 (a) at 2.68 GHz, strong current distributions are mainly concentrated on the surfaces of the stair-shaped monopoles, and this means the input energy is mainly radiated into the air by these monopoles. Therefore, the resonant frequency can be estimated by the length of the monopole, that is

$$f_1 \approx \frac{c}{4(L_1 + L_2 + L_3)\sqrt{\epsilon_{r1}}} \quad (1)$$

In Fig. 5 (b) at 2.18 GHz, strong current distributions are found on the edges of the four open slot. Slot radiation mode is excited at this frequency. So the resonant frequency can be estimated by

$$f_2 \approx \frac{c}{2(L_4 + L_5 + L_6)\sqrt{\epsilon_{r2}}} \quad (2)$$

In Fig. 5 (c) at 1.72 GHz, strong current distributions are mainly focused on the surface of the square patch. Therefore, patch mode is excited, and the resonance at this frequency is mainly determined by the square patch. The corresponding resonant frequency can be estimated by

$$f_3 \approx \frac{c}{2(2L_6 + w_3)\sqrt{\epsilon_{r3}}} \quad (3)$$

In equations (1)-(3),  $c$  is the light velocity in the free space, and  $\epsilon_{r1}$ ,  $\epsilon_{r2}$ , and  $\epsilon_{r3}$  are the effective dielectric permittivities for the monopoles, the slots, and the patch, respectively. Note that the collective current direction on the stair-shaped monopoles shown in Fig. 5 (a) and four open slots shown in Fig. 5 (b) is in the  $\varphi=+45^\circ$  direction, which is realized for the  $+45^\circ$  polarization. Whereas in the  $\varphi=-45^\circ$  direction, currents directions are opposite, and radiations from these opposite currents are cancelled in the far-field. Therefore, a low cross-polarization level can be expected for the proposed antenna.

To illustrate the effects of the different antenna parameters on the antenna performance of the different resonances, parameters of  $L_1$ ,  $L_4$ , and  $L_6$  are studied in Fig. 6 according to the equations in (1)-(3). As shown in Fig. 6 (a), when the length of the monopole  $L_1$  becomes longer, it can be observed that the monopole resonance at the higher frequency moves to lower frequency, whereas the other resonances almost keep unchanged. In Fig. 6 (b), when the length of the open slot ( $L_4$ ) grows longer, the slot mode at the center frequency also moves to lower frequency. The resonances for the monopole mode and the patch mode are almost unaffected.

When studying the parameter of  $L_6$  for the patch mode in Fig. 6 (c),

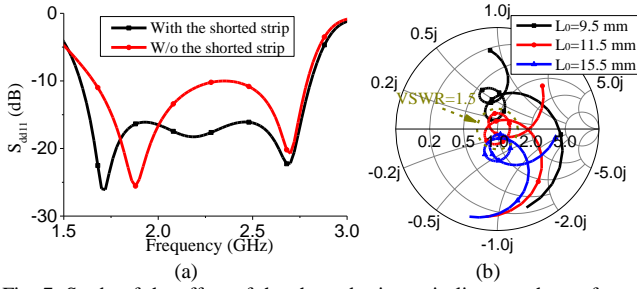


Fig. 7. Study of the effect of the shorted microstrip lines on the performance of the impedance bandwidth for Ant. 3. (a) With and without the shorted microstrip lines. (b) Variation as the length of the shorted microstrip lines.

the variation of the curves is a little complicated. As the increase of the length of  $L_6$ , the lower resonance for the patch mode moves to the lower frequency, while other resonances are affected by the change of  $L_6$ . The center resonance for the slot mode slightly shifts to the lower frequency due to the increase of the open slot length. The higher resonance for the monopole mode also shifts to the lower frequency due to the increase of the equivalent electric length for  $L_3$ , which is printed on the top of the patch. This can also be demonstrated by (1)-(3), when  $L_6$  is changed, both  $f_2$  and  $f_3$  are affected. Therefore, as the change of the patch mode, both the slot mode and the monopole mode will be affected.

#### D. Impedance Matching

To match the three different resonances well with characteristic impedance of the differentially fed coaxial cables, shorted microstrip lines are introduced to tune the input impedance of the antenna. Fig. 7 shows the effect of the shorted microstrip lines on the impedance bandwidth of the antenna. In Fig. 7 (a), when the shorted microstrip lines are removed from the antenna, it is observed that one reflection zero is disappeared on the curve with narrowed impedance bandwidth due to the mismatching between the antenna radiator and the feeding cables. Furthermore, the first reflection zero shifts to the upper frequency, and the reflection coefficient at the center band is also affected and deteriorated.

To extensively investigate the variation of the length of the shorted lines, different shorted strip length of  $L_0$  are studied. As shown in the smith chart in Fig. 7 (b), with the increase of the length, the inductance produced by the shorted microstrip line grows bigger. This means more inductance is shunted to the input port. Therefore, the smith curve is moved to the inverse direction of the inductive region as the increase of the length. As shown in the smith chart, when  $L_0$  is selected as 11.5 mm, a widest impedance bandwidth is obtained for the antenna, and the smith curve of Ant. 3 within the VSWR=1.5 circle is from 1.63GHz to 2.77 GHz.

#### E. Harmonic Suppression

Thanks to the center radiating patch, compact stepped impedance resonators can be elaborately integrated on the top of the patch. Fig. 8 shows the detailed configuration of the stepped impedance resonator. The stepped impedance resonator is composed of a high impedance microstrip line with the width of  $w_5$  and length of  $L_9$ , and a low impedance microstrip line with the width of  $w_4$  and length of  $L_8$ . By using the stepped impedance resonator, an elliptic function lowpass filter can be realized with two attenuation poles [21]-[22]. Fig. 9 shows the filtering response of the integrated lowpass filter. As shown in the figure, the simulated reflection coefficient from 1.7 GHz to 2.7 GHz is lower than -20 dB. Two attenuation poles are obtained at 4.5 GHz and 7 GHz. The simulated suppression for the lowpass filter from 4.1 GHz to 8.1 GHz is higher than 15 dB.

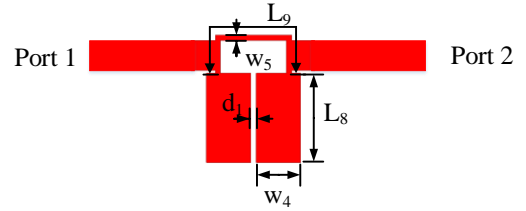


Fig. 8. Configuration of the stepped impedance resonator based lowpass filter. (Detailed parameters:  $L_8=5$  mm,  $L_9=8$  mm,  $w_4=2.5$  mm,  $d_1=0.3$  mm.)

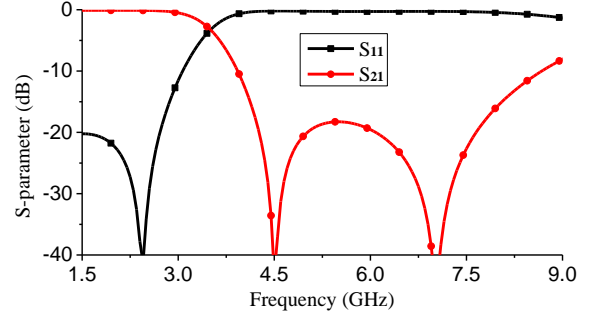


Fig. 9. Filter response of the stepped impedance resonator based lowpass filter.

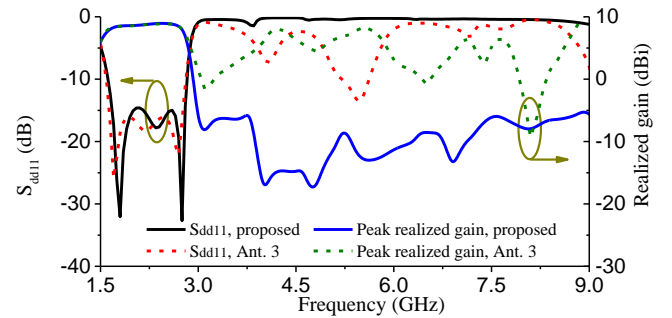


Fig. 10. Simulated  $S_{dd11}$  and peak realized gain of the proposed antenna and Ant. 3.

Fig. 10 compares the simulated  $S_{dd11}$  and peak realized gain of the proposed antenna with Ant. 3. As shown in the figure, Ant. 3 has many undesired resonances and radiations. Harmonic resonances of Ant. 3 can be observed at around 4.1 GHz, 5.5 GHz, 7.15, and 7.6 GHz. Correspondingly, the peak realized gains at these frequencies are found with high values, which are greater than 5 dBi. To reduce the antenna harmonic radiation, compact stepped impedance resonators are elaborately integrated into the proposed antenna without any increase of the antenna footprint. After the stepped impedance resonators are integrated into the antenna, the higher order harmonic resonances and radiations are greatly suppressed. Referring to the simulated results in Fig. 9, high suppression can be found at the frequencies of the two deep attenuation poles. Combining with the multi-resonance characteristic of Ant. 3, improved wideband harmonic suppression can be observed in this figure. Strong reflection is achieved from 3 GHz to 9 GHz for the antenna with the simulated  $S_{dd11} > -1.46$  dB. In addition, the gain over the whole harmonic frequency band is lower than -5.1 dBi. Three octave harmonic suppression is achieved by elaborately integrating the stepped impedance resonators into the antenna.

### III. RESULTS AND DISCUSSION

#### A. Antenna Verification

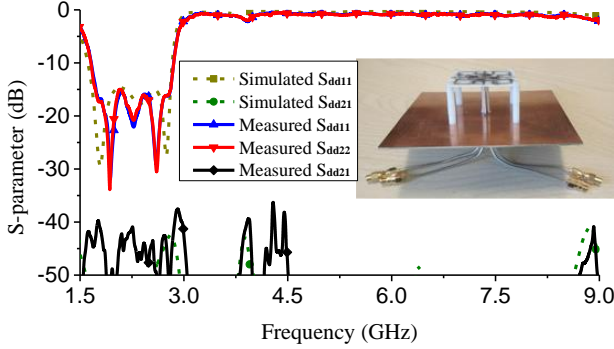


Fig. 11. Measured and simulated S-parameters of the proposed differentially fed dual-polarized antenna.

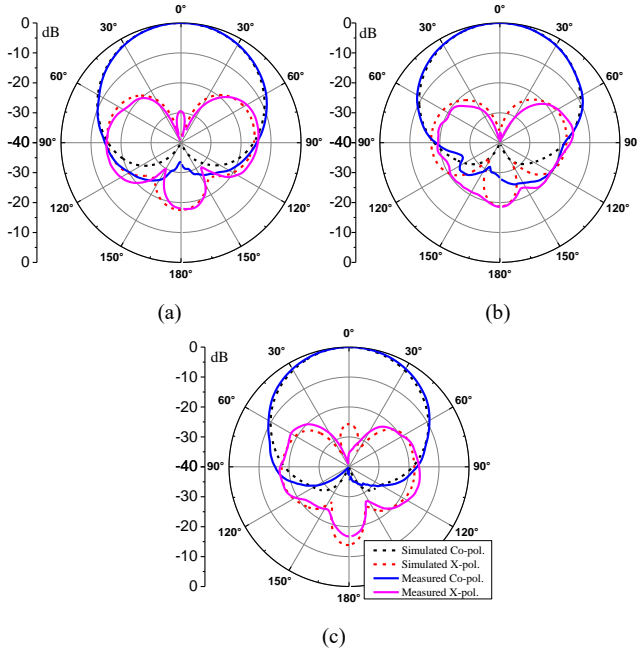


Fig. 12. Measured and simulated normalized radiation patterns of the proposed antenna in H-plane when differential port d1 is excited.

The proposed differentially fed dual-polarized antenna was fabricated and measured at the University of Kent. The photograph of the fabricated prototype of the antenna is inset into the right of the Fig. 11. In the figure, both the measured and simulated S-parameters of the prototype are shown for a good comparison. The measured impedance bandwidth for  $S_{dd11}$  and  $S_{dd22}$  lower than -15 dB is from 1.70 GHz to 2.81 GHz. Owing to the symmetry of the antenna, very high isolation is measured within the whole operation band, which is higher than 39 dB. Furthermore, three octave high harmonic suppression is achieved with the measured  $S_{dd11}$  and  $S_{dd22}$  higher than -2.2 dB from 3 GHz to 9 GHz. Good agreement can be observed between the simulated and measured results. Small differences between the simulated and measured results are mainly caused by the fabrication and solder errors of the feed cables.

Fig. 12 shows the measured and simulated normalized H-plane radiation patterns when differential port d1 is excited at 1.7 GHz, 2.2 GHz, and 2.7 GHz. Owing to the symmetry of the antenna, only H-plane radiation patterns are given in the figure. As can be seen in the figure, the measured radiation patterns agree well with the simulated radiation patterns. The measured cross-polarization level is 29 dB lower than co-polarization in the broadside direction and 23 dB lower in the  $\pm 30^\circ$  directions. The measured front to back ratio is

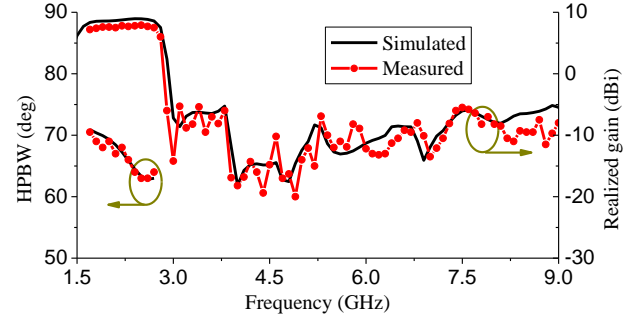


Fig. 13. Measured and simulated HPBW and peak realized gain of the proposed differentially fed dual-polarized antenna.

TABLE I  
COMPARISON OF THE REFERENCE ANTENNAS

Ref.	Bandwidth	Height	Isolation (dB)	$S_{11}$ of the Harmonic	Gain of the Harmonic Radiation
[12]	52% 1.7-2.9 GHz	$0.27\lambda_0$	36.3	N.G.	N.G.
[13]	48% 1.68-2.74 GHz	$0.24\lambda_0$	35	N.G.	N.G.
[14]	45% 1.7-2.75 GHz	$0.3\lambda_0$	38	N.G.	N.G.
[15]	45% 1.71-2.69 GHz	$0.4\lambda_0$	39	N.G.	N.G.
[23]	7%	0.508 mm	/	>-2.5 dB 3.5-12 GHz	N.G.
[24]	8.4%	1.57 mm	/	>-2.5 dB 5.2-13 GHz	N.G.
[25]	8.42%	0.8 mm	/	>-2.8 dB 3-10 GHz	N.G.
[26]	13.9%	1.8 mm	/	>-4.2 dB 3-9 GHz	N.G.
This work	49% 1.70-2.81 GHz	$0.25\lambda_0$	39	>-2.2 dB 3-9 GHz	<-5.3 dBi 3-9 GHz

higher than 16 dB. Fig. 13 shows the measured HPBW and peak realized gain of the antenna. The measured HPBW varies from  $63^\circ$  to  $71^\circ$  within the half-power bandwidth. Stable antenna gain is also achieved within the bandwidth, which varies from 7.2 dBi to 7.9 dBi. Most importantly, wideband harmonic radiations from 3 GHz to 9 GHz are suppressed with the maximum harmonic gain lower than -5.3 dBi.

### B. Comparison

Table I compares the presented antenna with the recently published antennas. In the table,  $\lambda_0$  is the free space wavelength at the center operation frequency. Dual-polarized antennas in [12]-[15] are designed for 1.7-2.7 GHz base station applications by using crossed dipoles, dual-dipoles, or the multi-dipoles for wideband operations. Note that the antenna in [15] has the highest port isolation, but its profile is also the largest. As the development of the wireless communication systems, more and more military and commercial wireless devices are increased in the realistic environment. If the harmonic radiations are not considered, serious interferences and congestions will be caused to affect each other's operation. To the authors' knowledge, few of these base station antennas are concerned about the harmonic radiations.

Designs in [23]-[26] are the single-polarized antennas, so there are no port isolations. For the harmonic suppression, normally only

reflection coefficients are considered, so the harmonic radiations are not provided in the references. Designs in [23]-[24] are the narrow band patch antennas. By introducing a pair of partial ring slots and an open-ended circular stub under the microstrip line [23], wideband harmonic suppression is achieved. However, additional footprint is required for these additional feed network. Designs in [25]-[26] are the slot antennas, and different shaped etched slots are employed as the defected ground structures to achieve the wideband harmonic suppression. Regarding the wideband antennas for base station applications, multiple resonances are normally employed to broaden the impedance bandwidth. Therefore, compared to the narrow band antennas in [23]-[26], more complicated harmonic radiations will be appeared at the upper out-of-band, and it is more difficult to realize wideband antennas with wideband harmonic suppression. As for the presented antenna, wide impedance bandwidth of 1.70-2.81 GHz (49%) is achieved for  $S_{dd11}$  and  $S_{dd22}$  lower than -15 dB with high isolation (>39 dB). Moreover, wideband harmonic suppression from 3 GHz to 9 GHz is obtained with the  $S_{dd11}$  and  $S_{dd22}$  higher than -2.2 dB. In addition, the corresponding measured harmonic radiation gain is lower than -5.3 dBi.

#### IV. CONCLUSION

This communication presents a novel wideband differentially fed dual-polarized antenna with wideband harmonic suppression for base station applications. The wide impedance bandwidth is obtained by combing different resonances from slots, monopoles, and a patch. Symmetrical radiation patterns and low cross-polarization levels are obtained by etching eight symmetrical open slots and the differential fed method. By properly changing the length of the shorted stubs, three different resonances are well matched to the feeding cables. To suppress the harmonic radiation of the antenna, compact stepped impedance resonators are elaborately integrated on the top of the patch with wideband harmonic suppression and without any increase of the antenna footprint. The antenna prototype was fabricated and measured for verification. The measured results demonstrated that wide impedance bandwidth of 1.70-2.81 GHz for  $S_{dd11} < -15$  dB is achieved with high port isolation of 39 dB. Moreover, wideband harmonic suppression from 3 GHz to 9 GHz is obtained with the  $S_{dd11} > -2.2$  dB and the harmonic gain  $< -5.3$  dBi. Stable gain and radiation patterns are also achieved within the bandwidth. Therefore, the proposed antenna can be a good candidate for base station applications with excellent wideband harmonic suppressions.

#### REFERENCES

- [1] S.-C. Gao, L.-W. Li, M.-S. Leong, and T.-S. Yeo, "Dual-polarized slot coupled planar antenna with wide bandwidth," *IEEE Trans. Antennas Propag.*, vol. 51, no. 3, pp. 441-448, Mar. 2003.
- [2] S. Gao, L. W. Li, M. S. Leong, and T. S. Yeo, "A broad-band dual-polarized microstrip patch antenna with aperture coupling," *IEEE Trans. Antennas Propag.*, vol. 51, no. 4, pp. 898-900, Apr. 2003.
- [3] Z. Tang, J. Liu, Y. Cai, J. Wang and Y. Yin, "A wideband differentially fed dual-polarized stacked patch antenna with tuned slot excitations," *IEEE Trans. Antennas Propag.*, vol. 66, no. 4, pp. 2055-2060, April 2018.
- [4] K. S. Ryu and A. A. Kishk, "Wideband dual-polarized microstrip patch excited by hook shaped probes," *IEEE Trans. Antennas Propag.*, vol. 56, no. 12, pp. 3645-3649, Dec. 2008.
- [5] Y. Guo, K. Khoo and L. C. Ong, "Wideband dual-polarized patch antenna with broadband baluns," *IEEE Trans. Antennas Propag.*, vol. 55, no. 1, pp. 78-83, Jan. 2007.
- [6] C. Deng, Y. Li, Z. Zhang and Z. Feng, "A wideband high-isolated dual-polarized patch antenna using two different balun feedings," *IEEE Antennas Wireless Propag. Lett.*, vol. 13, pp. 1617-1619, 2014.
- [7] X. Yang, L. Ge, J. Wang and C. Sim, "A differentially driven dual-polarized high-gain stacked patch antenna," *IEEE Antennas Wireless Propag. Lett.*, vol. 17, no. 7, pp. 1181-1185, July 2018.
- [8] C. R. White and G. M. Rebeiz, "A differential dual-polarized cavity-backed microstrip patch antenna with independent frequency tuning," *IEEE Trans. Antennas Propag.*, vol. 58, no. 11, pp. 3490-3498, Nov. 2010.
- [9] H. Nawaz and I. Tekin, "Dual-polarized, differential fed microstrip patch antennas with very high interport isolation for full-duplex communication," *IEEE Trans. Antennas Propag.*, vol. 65, no. 12, pp. 7355-7360, Dec. 2017.
- [10] N. Liu, L. Zhu, X. Zhang and W. Choi, "A wideband differential-fed dual-polarized microstrip antenna under radiation of dual improved odd-order resonant modes," *IEEE Access*, vol. 5, pp. 23672-23680, 2017.
- [11] N. Liu, L. Zhu, W. Choi and J. Zhang, "A low-profile differentially fed microstrip patch antenna with broad impedance bandwidth under triple-mode resonance," *IEEE Antennas Wireless Propag. Lett.*, vol. 17, no. 8, pp. 1478-1482, Aug. 2018.
- [12] D. Wen, D. Zheng and Q. Chu, "A wideband differentially fed dual-polarized antenna with stable radiation pattern for base stations," *IEEE Trans. Antennas Propag.*, vol. 65, no. 5, pp. 2248-2255, May 2017.
- [13] Z. Tang, J. Liu and Y. Yin, "Enhanced cross-polarization discrimination of wideband differentially fed dual-polarized antenna via a shorting loop," *IEEE Antennas Wireless Propag. Lett.*, vol. 17, no. 8, pp. 1454-1458, Aug. 2018.
- [14] Y. Cui, X. Gao and R. Li, "A broadband differentially fed dual-polarized planar antenna," *IEEE Trans. Antennas Propag.*, vol. 65, no. 6, pp. 3231-3234, June 2017.
- [15] Y. Luo and Q. Chu, "Oriental crown-shaped differentially fed dual-polarized multidipole antenna," *IEEE Trans. Antennas Propag.*, vol. 63, no. 11, pp. 4678-4685, Nov. 2015.
- [16] L. Ge and K. M. Luk, "A magneto-electric dipole antenna with low-profile and simple structure," *IEEE Antennas Wireless Propag. Lett.*, vol. 12, pp. 140-142, 2013.
- [17] Q. Xue, S. W. Liao and J. H. Xu, "A differentially-driven dual-polarized magneto-electric dipole antenna," *IEEE Trans. Antennas Propag.*, vol. 61, no. 1, pp. 425-430, Jan. 2013.
- [18] Z. L. Ma and C. H. Chan, "Waveguide-based differentially fed dual-polarized magnetoelectric dipole antennas," *IEEE Trans. Antennas Propag.*, vol. 65, no. 8, pp. 3849-3857, Aug. 2017.
- [19] V. Radisic, Y. Qian and T. Itoh, "Novel architectures for high-efficiency amplifiers for wireless applications," *IEEE Trans. Microw. Theory Tech.*, vol. 46, no. 11, pp. 1901-1909, Nov. 1998.
- [20] E. Babakrpur and W. Namgoong, "A dual-path 4-phase nonuniform wideband receiver with digital mmse harmonic rejection equalizer," *IEEE Trans. Microw. Theory Tech.*, vol. 65, no. 2, pp. 386-395, Feb. 2017.
- [21] L.-H. Hsieh and K. Chang, "Compact elliptic-function low-pass filters using microstrip stepped-impedance hairpin resonators," *IEEE Trans. Microw. Theory Tech.*, vol. 51, no. 1, pp. 193-199, Jan. 2003.
- [22] J. T. Ku, M. J. Maa, and P. H. Lu, "A microstrip elliptic function filter with compact miniaturized hairpin resonator," *IEEE Microw. Guided Wave Lett.*, vol. 10, pp. 94-95, Mar. 2000.
- [23] S. Biswas, D. Guha and C. Kumar, "Control of higher harmonics and their radiations in microstrip antennas using compact defected ground structures," *IEEE Trans. Antennas Propag.*, vol. 61, no. 6, pp. 3349-3353, June 2013.
- [24] J. Zhang, L. Zhu, Q. Wu, N. Liu and W. Wu, "A compact microstrip-fed patch antenna with enhanced bandwidth and harmonic suppression," *IEEE Trans. Antennas Propag.*, vol. 64, no. 12, pp. 5030-5037, Dec. 2016.
- [25] C. Sim, M. Chang and B. Chen, "Microstrip-fed ring slot antenna design with wideband harmonic suppression," *IEEE Trans. Antennas Propag.*, vol. 62, no. 9, pp. 4828-4832, Sept. 2014.
- [26] W. Li, Y. Wang, B. You, Z. Shi and Q. H. Liu, "Compact ring slot antenna with harmonic suppression," *IEEE Antennas Wireless Propag. Lett.*, vol. 17, no. 12, pp. 2459-2463, Dec. 2018.